JOURNAL OF GEOPHYSICAL RESEARCH, VOL. 112, D12S18, doi:10.1029/2006JD007777, 2007

Biomass burning and pollution aerosol over North America: Organic components and their influence on spectral optical properties and humidification response

A. Clarke,[1] C. McNaughton,[1] V. Kapustin,[1] Y. Shinozuka,[1] S. Howell,[1] J. Dibb,[2] J. Zhou,[1] B. Anderson,[3] V. Brekhovskikh,[1] H. Turner,[4] and M. Pinkerton[1]

Received 11 July 2006; revised 5 April 2007; accepted 19 April 2007; published 9 June 2007.

[1] Thermal analysis of aerosol size distributions provided size resolved volatility up to temperatures of 400°C during extensive flights over North America (NA) for the INTEX/ICARTT experiment in summer 2004. Biomass burning and pollution plumes identified from trace gas measurements were evaluated for their aerosol physiochemical and optical signatures. Measurements of soluble ionic mass and refractory black carbon (BC) mass, inferred from light absorption, were combined with volatility to identify organic carbon at 400°C (VolatileOC) and the residual or refractory organic carbon, RefractoryOC. This approach characterized distinct constituent mass fractions present in biomass burning and pollution plumes every 5–10 min. Biomass burning, pollution and dust aerosol could be stratified by their combined spectral scattering and absorption properties. The ''nonplume'' regional aerosol exhibited properties dominated by pollution characteristics near the surface and biomass burning aloft. VolatileOC included most water-soluble organic carbon. RefractoryOC dominated enhanced shortwave absorption in plumes from Alaskan and Canadian forest fires. The mass absorption efficiency of this RefractoryOC was about 0.63 $m^2\ g^{-1}$ at 470 nm and 0.09 $m^2\ g^{-1}$ at 530 nm. Concurrent measurements of the humidity dependence of scattering, γ, revealed the OC component to be only weakly hygroscopic resulting in a general decrease in γ with increasing OC mass fractions. Under ambient humidity conditions, the systematic relations between physiochemical properties and γ lead to a well-constrained dependency on the absorption per unit dry mass for these plume types that may be used to challenge remotely sensed and modeled optical properties.

Citation: Clarke, A., et al. (2007), Biomass burning and pollution aerosol over North America: Organic components and their influence on spectral optical properties and humidification response, *J. Geophys. Res.*, *112*, D12S18, doi:10.1029/2006JD007777.

1. Introduction

[2] The importance of aerosol physical, chemical and optical properties and their role in regional and global climate forcing is well recognized. Yet there remains considerable uncertainty about the contribution of both natural and anthropogenic aerosols to their overall radiative effects [*Bates et al.*, 2006]. Some uncertainty is due to the complex and varied properties of organic aerosols and more information is needed to better model their optical properties [*Kanakidou et al.*, 2004]. Key properties from a climate and radiative perspective are the size distribution, light scattering and light absorption coefficients, their wavelength dependence and their hygroscopic properties. The latter controls the uptake of water, ambient aerosol optical properties and activation in clouds. The extent to which organic aerosol are internally or externally mixed with other aerosol types is also an important determination. Given the thousands of organic species and their diverse characteristics, a means for generalizing relevant properties is desirable. One commonly identified grouping is the water soluble organic carbon (WSOC) recently measured aboard research aircraft [*Weber et al.*, 2001].

[3] The light absorption coefficient, $\sigma_{ap,}$ is a radiatively important aerosol property. There is a long history of measuring light absorbing carbon (LAC) and black carbon (BC), often associated with soot; and yet significant uncertainties remain and differences exist in fundamental properties like the mass absorption coefficient (MAE) or refractive index and best ways to report them [*Bond and Bergstrom*, 2006]. The recognition that organic carbon (OC)

[1]School of Ocean and Earth Science and Technology, University of Hawaii, Honolulu, Hawaii, USA.
[2]Institute for the Study of Earth, Oceans, and Space, University of New Hampshire, Durham, New Hampshire, USA.
[3]NASA Langley Research Center, Hampton, Virginia, USA.
[4]Department of Chemical Engineering, University of Alabama, Tuscaloosa, Alabama, USA.

0148-0227/07/2006JD007777$09.00

aerosol can absorb appreciably, particularly at shorter wavelengths [*Kirchstetter et al.*, 2004], has refocused attention on light absorbing properties of this so-called "brown carbon" and the need for multiwavelength measurements [*Andreae and Gelencser*, 2006]. Measurements of MAE for OC aerosol from typical sources are rare but provide an important tool for models that carry OC mass and use it to estimate aerosol optical effects.

[4] Recently, so-called Humic Like Substances (HULIS) have been suggested as a major component of absorbing OC. Humic substances include fulvic acid (water soluble), humic acid (base soluble) and humin (insoluble) components [*Graber and Rudich*, 2006]. HULIS also includes both water soluble and insoluble fractions. However, most studies have focused upon the water soluble fraction or fulvic acid component and not the humic acid or insoluble humin found to be more absorbing in the shorter wavelengths [*Graber and Rudich*, 2006]. These authors also suggest transformation of OC components can occur in the atmosphere over time and large uncertainties exist regarding the various sources, transformations and properties of both soluble and insoluble components. However, other fuels like propane combustion have been found to generate a more aromatic OC aerosol that increases with C/O ratios in the burner. This OC is considered to arise from long chained PAH and was found to have much greater shortwave absorption relative to the soot (BC) component [*Schnaiter et al.*, 2006]. Other studies have also found that burning of lignite coal can yield enhanced shortwave absorption indicative of coal tar or incompletely aromatized carbon [*Bond et al.*, 1999b].

[5] The water uptake by aerosol must be quantified to correctly calculate or model optical effects under actual atmospheric conditions. Recent evaluations of aerosol humidity-dependent growth demonstrate the influence of OC in suppressing aerosol growth compared to that of common ionic species alone [*Quinn et al.*, 2005]. Although OC may suppress aerosol growth, the presence of WSOC may enhance the nucleating properties of some insoluble aerosols (such as dust) and making them more effective cloud condensation nuclei [*Mayol-Bracero et al.*, 2002b]. Hence OC properties can influence both the direct and indirect radiative effects of aerosol.

2. Aircraft Measurements

2.1. Aircraft Inlet Sampling Performance

[6] Our data is part of the extensive airborne data set from the NASA INTEX-NA experiment taken aboard the DC-8 [*Singh et al.*, 2006]. The University of Hawaii (UH) solid diffuser inlet was used to sample in situ aerosol size distributions and optical properties aboard the NASA DC-8 [*McNaughton et al.*, 2007]. Aerosol filter samples were measured for bulk-chemistry behind the University of New Hampshire (UNH) solid diffuser inlet. Inlet performance during the 2003 DC-8 Inlet Comparison Experiment (DICE) demonstrated that the UH and UNH inlets perform similarly while sampling both supermicrometer sea salt at high (80–95%) relative humidity and supermicrometer mineral dust in desert environments[*McNaughton et al.*, 2007]. Comparisons with ground based instrumentation show that the UH and UNH inlets and transport system pass particles with aerodynamic diameters of 5 μm with better than 50% efficiency. Significant dust was infrequent and aerosol optical properties were typically dominated by smaller particle sizes. Hence we conclude that the DC-8 inlets effectively sampled the aerosol dominating the surface area and optical effects during INTEX-NA.

2.2. Thermally Resolved Aerosol Size Distributions

[7] A modified Particle Measurement Systems (PMS, Boulder, Colorado) laser optical particle counter (OPC, 632 nm) was used to measure the dry (RH < 30%), optically effective aerosol size distribution between 0.1 μm and 5 μm every 3 s [*Clarke et al.*, 2004]. The He-Ne OPC laser (632 nm) detects light scattered by individual particles over 35–145°. Dry size distributions were ensured by mixing sample air with an equal flow of desiccated filtered air. This minimizes size and particle refractive index variability due to water uptake and thereby reduces OPC measurement errors. The OPC was calibrated before during and after deployment using a combination of National Institute of Standards and Technology (NIST) traceable polystyrene, silica, and borosilicate glass microspheres(Duke Scientific). Since the OPC measures optically effective sizes (D_{oe}) the data is well suited to modeling aerosol optical properties. Linear regression of total and submicrometer scattering calculations from the size distributions compared to measured scattering values gives a slope of 0.91 and a correlation coefficient, r^2, 0.95 [*Shinozuka et al.*, 2007].

[8] The OPC operates in series with a redesigned thermo-optical aerosol discriminator (TOAD) [*Clarke*, 1991] with a 400°C temperature channel added to the original 40°, 150° and 300°C (later increased to 350°C). Peak temperatures were measured by a thermocouple in the center of the airflow. The TOAD cycles between temperature channels every 30 s during horizontal flight legs. This results in thermo-optical characterization of the optically effective size range every 2 min. During vertical profiles the OPC does not cycle between temperatures. At a typical DC-8 ascent/descent rate of 450 m min^{-1} this usually gives a vertical resolution of 25 m for submicrometer size distributions. Larger particle sizes require longer averaging due to lower count statistics.

[9] Volatility data was interpreted in conjunction with inorganic ionic compositions measured on filter samples using ion chromatography as described elsewhere [*Dibb et al.*, 2003]. These generally limited the time periods used here as they were exposed for 5–10 min below 6 km and somewhat longer aloft. These filters were usually analyzed within 24 hours.

2.3. Aerosol Optical Properties and Humidity Dependence

[10] Total and submicrometer aerosol light scattering ($\sigma_{sp,\ tot}$, $\sigma_{sp,\ sub}$) was measured at 450, 550, and 700 nm wavelengths using two TSI model 3563 integrating nephelometers [*Anderson et al.*, 1996; *Heintzenberg and Charlson*, 1996] corrected according to [*Anderson and Ogren*, 1998]. The submicrometer TSI nephelometer employed a 1 μm aerodynamic impactor maintained at 30 lpm using an Alicat Scientific volumetric flow controller. Sample air residence time inside the nephelometers was less than 10 s and the instrument relative humidity (RH) is typically less than 30%. Two single-wavelength (λ = 540 nm) Radiance Research

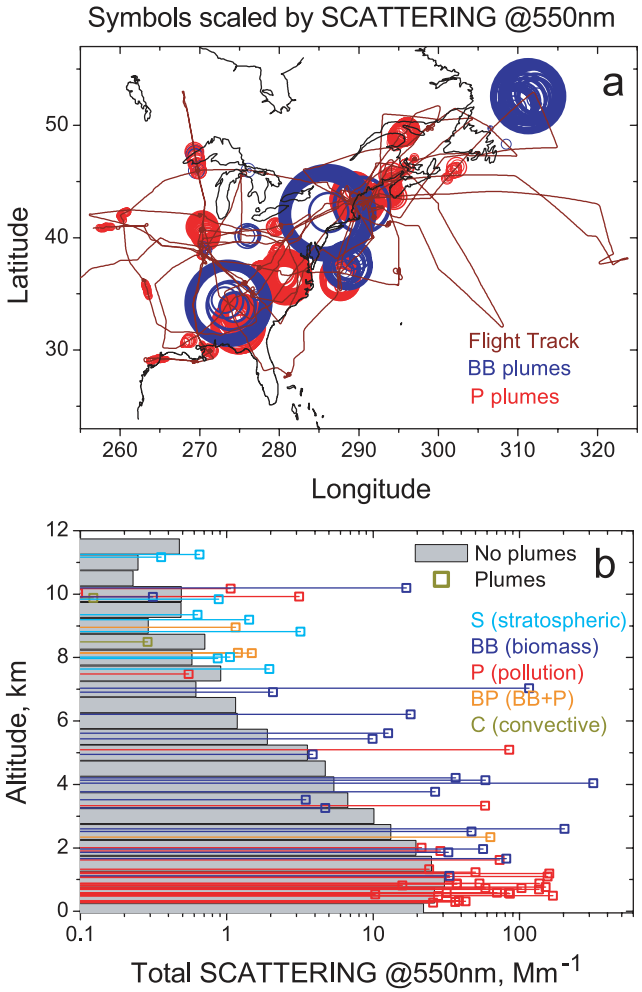

Figure 1. (a) Map of North America showing DC-8 flight routes (thin lines) and plume locations (circles) where diameters are proportional to 60 s measured light scattering at 530 nm. (b) Vertical profile of measured scattering for plume types identified and the average of all nonplume data as a function of altitude during INTEX-NA. See text for plume characterization strategy.

model M903 nephelometers operated in parallel providing a direct measurement of the increase in light scattering as a function of relative humidity [*Howell et al.*, 2006a]. The humidified nephelometer operated at 80% RH while the dry nephelometer RH was maintained below 40%. Temperature and relative humidity were measured using Vaisala RH & T sensors (manufacturer stated accuracy ±2% RH and ±0.1°C) mounted in the RR nephelometer sample outlet without their protective sheath to improve response time. This measurement provides a two point measurement that can be fit to express the growth response, γ, of the scattering, σ, using equation (1) [*Quinn et al.*, 2005].

$$\delta_{wet} = \delta_{dry} \cdot \left[\frac{\left(1 - \frac{RH_{dry}}{100}\right)}{\left(1 - \frac{RH_{wet}}{100}\right)} \right]^{\gamma} \quad (1)$$

[11] During INTEX-NA a new three-wavelength particle soot absorption photometer (PSAP, Radiance Research) was provided by David Covert (University of Washington) to measure aerosol light absorption at 470, 530, 660 nm wavelengths. There is not yet a consensus in the literature about the best methods for correcting this new instrument for multiple scattering and loading artifacts. We have chosen to use the corrections modified for the other channels using wavelength dependence of the scattering correction factor "s" from *Virkkula et al.* [2005]. There is some discrepancy between these corrections and those of a 1 wavelength PSAP [*Bond et al.*, 1999a] resulting in about 25% lower absorption than measured with single wavelength PSAPs. The reason for the discrepancy is not clear, but there are a few possibilities: the light source and optical path in the PSAP was somewhat different; the tested particles were all either nonabsorbing or very strongly absorbing, making them poor models for the high single-scatter albedo experienced during INTEX-NA; or particle loadings were much higher than we experienced. Other soot studies and comparisons are underway to resolve these differences (D. Covert, personal correspondence, unpublished results, 2006). These differences will not affect the general behavior and properties discussed in this paper.

3. INTEX-NA Plumes

[12] Plumes from North America biomass burning sources can evolve and mix with continental pollution plumes and diffuse sources to contribute to regional pollution outflow from North America [*Li et al.*, 2005]. Repeated encounters with diverse plumes aloft during INTEX-NA [*Singh et al.*, 2006] provide a statistical characterization of their chemistry, physics and optical properties. Background concentrations of various signature species such as CO, O_3, NO_2, SO_2, HCN, C_3H_8, and C_2H_2 were established by dividing the measurements into 1-km altitude bins and creating vertical profiles of each species. A plume encounter was identified when one of the tracer species exceeded the 95th percentile of the measured values within a given altitude region. 84 plumes were detected this way and characterized as biomass burning (BB) or pollution (P). These plumes represent about 24 hours of flight time or about 17% of the research hours flown. The remaining measurements are referred to here as nonplume cases. In order to facilitate the classification, 10-day back trajectories were analyzed for each plume. BB plumes were associated with high levels of HCN, CO, ethyne, absorption, and CH_3CN. P plumes were associated with high concentrations of O_3, CO, alkanes, SO_2, NMHC, and ultrafine condensation nuclei (3–3000 nm). Some plumes reflect a mix of plume and nonplume air encountered over a given leg. This classification is available on the NASA INTEX-NA archive (ftp://ftp-air.larc.nasa.gov/pub/INTEXA/MERGES/DC8/1_MINUTE/). The number of data points for P and BB plumes in the following plots vary depending upon the availability of concurrent data being compared.

[13] The spatial distribution of these plumes is shown as circles for our 60 s data collected over eastern NA superimposed on the flight tracks (thin lines, Figure 1a). The size of the circles is proportional to the 60 s average light scattering values. These plumes are also evident in flight leg average values averaged over 250 m altitude bins in

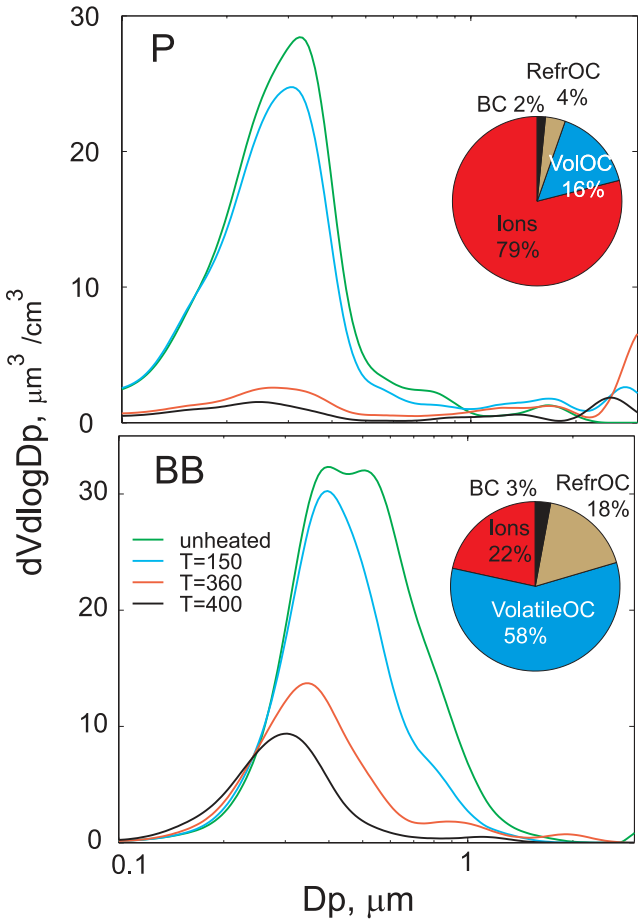

Figure 2. Examples of OPC size distributions with the results of heating aerosol to indicated temperatures for (top) a pollution plume case and (bottom) a biomass burning aerosol case. The mean size and the refractory fraction remaining at 400°C is much greater for biomass burning aerosol. The pie chart insets illustrate the components described in text.

Figure 1b and shown as horizontal lines superimposed upon the grey "nonplume" background. Below 1 km the plumes were exclusively identified as pollution. The total number of BB and P plumes are similar in the 1–3 km altitude, a region that includes most active exchange between the boundary layer and free troposphere. From 3–7 km most plumes identified by exceeding the 95th percentile are BB plumes identified as originating in Alaska and western Canada. At higher altitudes, isolated dilute plumes of either type are present which include deep convection over the continent in summer and some intrusions of stratospheric air.

4. Thermal Analysis and Aerosol Carbon

[14] Our thermal treatment provides information on the size-resolved volatility of the aerosol components, state of mixing and the residual refractory component remaining at the highest temperature used. Refractory materials remaining at high temperature (400°C) include dust, fly ash, black carbon (BC, soot) and some OC components. Organic and elemental carbon measurements using thermal evolved gas analysis in air provide an opportunity to examine the effects of thermal treatment on particulate carbon. It is now clear that some OC evolves over a range of temperatures that overlap those at which BC evolves [*Andreae and Gelencser*, 2006; *Bond and Bergstrom*, 2006; *Mayol-Bracero et al.*, 2002b]. BC may oxidize at temperatures below 450°C depending upon origin, state of mixing and aging, but these references indicate that at 400°C, very little BC is lost while much of the OC is gone. Henceforth we refer to the fraction of OC lost during heating to 400°C as VolatileOC, while that remaining we identify as RefractoryOC.

[15] A common assumption has been that soot is the only significant light absorbing form of carbon in atmospheric aerosol. However, the papers above (and references therein) discuss at length how some of the aerosol OC is also light absorbing, in addition to aerosol BC, and suggest the term light absorbing carbon (LAC) for the possible mixtures of these components. Laboratory samples of lignin and humic acid (two materials believed to be similar to those found in some aerosols) were shown to have multiple peaked structure in their thermal evolution up to temperatures of 700°C [*Andreae and Gelencser*, 2006]. Enhanced light absorption at shorter wavelengths is characteristic of these and other HULIS such as those observed in biomass-burning aerosols over the Amazon [*Hoffer et al.*, 2005].

[16] In order to clarify our thermal approach we reference the observations shown in the papers by *Kirchstetter et al.* [2004] and *Mayol-Bracero et al.* [2002a]. *Kirchstetter et al.* [2004] show the thermally evolved CO_2 before and after extraction of the samples using acetone to remove acetone soluble OC. *Mayol-Bracero et al.* [2002a] show the change in absorption concurrent with the evolution of CO_2. These measurements include biomass burning, pollution and diesel exhaust. Peaks in evolved CO_2 as a function of temperature correspond, in diesel exhaust cases, with light absorbing aerosol near 400–500°C. Diesel soot is a common LAC that is high in BC and it has been found to combust over a narrow temperature range between 470°C and 510°C [*Wittmaack*, 2005]. However, there is evidence that mixing with other inorganic species and aerosol aging can catalyze oxidation [*Andreae and Gelencser*, 2006] and shift thermal evolution to lower temperatures by as much as 100°C [*Novakov and Corrigan*, 1995] in response to the presence of metals such as Na^+ or K^+. These diverse measurements demonstrate that OC can evolve at many temperatures including those associated with BC (a) and that the temperature where absorbing BC can evolve can vary with sources, composition, state of mixing, trace metals etc.

5. Aerosol Composition and Thermal Volatility

[17] Our thermal analysis of volatility [*Clarke et al.*, 2004] was originally developed for clean marine regions where sea salt, sulfates and low mass fractions (ca. 15%) of organic components typically characterize the aerosol [*Clarke*, 1991]. Recent development of fast measurements (ca. 1 min) of soluble ions [*Weber et al.*, 2001] enabled us to extend our interpretation of volatility to the more chemically complex aerosols in polluted areas [*Clarke et al.*, 2004; *Howell et al.*, 2006b].

[18] Although BB and P plumes (Figure 1) are identified primarily by gas phase measurements, the plumes also differ in aerosol properties, including their volatility. Figure 2

shows examples of the effect of thermal heating to 40°C, 150°C, 360°C and 400°C on the volume distributions for a representative P and BB plumes. In this paper only unheated and 400°C heated volumes will be used. For the remainder of this paper, aerosol mass fractions derived from the thermally resolved size distributions are based on the following assumptions.

[19] 1. Accumulation mode pollution aerosol is internally mixed, as generally observed after several hours of aging using our thermal Tandem Differential Mobility Analyzer (unpublished INTEX-NA data) and in other polluted regions [*Clarke et al.*, 2004].

[20] 2. Supermicron particles contain little of the soluble inorganic ions. The nephelometers showed that coarse particles contributed significantly to scattering only about 10% of the time during INTEX-NA and absorption was dominated by small particles.

[21] 3. Particulate volumes calculated from OPC size distributions are representative. Optical sizing errors are primarily due to refractive index differences between the sampled particles and the calibration spheres (which have n = 1.588). As mentioned above, the desiccated dilution air serves to reduce water in the particles, increasing refractive index but reducing its variability, both of which suppress sizing errors. Remote sensing of biomass plumes over the east coast yielded a refractive index of 1.55 at 670 nm [*Colarco et al.*, 2004] and 1.54 for Indian pollution [*Müller et al.*, 2003] at 532 nm. Hence, since particle refractive index probably remained below 1.588 for normal pollution, OPC volumes may be systematically underestimated. Good agreement (within about 10%) between scattering calculated from size distributions and measured by nephelometers [*Shinozuka et al.*, 2007] provides confidence that the size distributions are realistic and we expect calculated volumes to be no more than 20% low. This would make little difference in the arguments that follow.

[22] 4. Submicrometer aerosol components volatile below 400°C include all measured soluble ions [*Dibb et al.*, 2003] along with any volatile organic carbon (VolatileOC). We estimate VolatileOC mass by subtracting the volume of measured ions from total volatile volume and assigning a density of 1.3 g cm^{-3} for the remaining VolatileOC volume. This is based upon a suggested range of 1.2 to 1.4 g cm^{-3} for organic aerosol [*Stelson*, 1990; *Turpin and Lim*, 2001] and a reported value of 1.4 g cm^{-3} for biomass smoke [*Reid et al.*, 2005]. We expect the VolatileOC density to be less than that of BC and RefractoryOC in smoke.

[23] 5. Aerosol volume (mass) remaining at 400°C includes refractory organic carbon (RefractoryOC) and absorbing black carbon (BC). The BC inferred from absorption (InferredBC) is based on a nominal mass absorption efficiency (MAE) of 10 m^2 g^{-1} at 550 nm. We have argued previously for a value near 7.5 m^2 g^{-1} at 550 nm [*Clarke et al.*, 2004], consistent with a recent survey of likely values [*Bond and Bergstrom*, 2006]. However, we use the higher value here in order to allow for a possible optical enhancement due to other internally mixed components [*Bond et al.*, 2006; *Fuller et al.*, 1999]. As shown below, the relative mass of BC is small so the resulting uncertainty has little effect on inferred OC.

[24] 6. We use volume based mixing rules with component densities of 1.8 g cm^{-3} for the refractory BC [*Fuller et al.*, 1999]. We are not aware of density data for RefractoryOC and use a value of 1.5 g cm^{-3} for bulk HULIS [*Hoffer et al.*, 2004] as we expect RefractoryOC density to be greater than VolatileOC but less than BC.

[25] 7. We use a mean density of ionic components of about 1.75 g cm^{-3} [*McMurry et al.*, 2002; *Stelson*, 1990] and assume any potential interaction between mixed components does not influence their effective density.

[26] 8. RefractoryOC volume is computed as the volume remaining at 400°C less the volume of inferred BC (i.e., area under the black curve in Figure 2 less the volume of inferred BC).

[27] In this manner we resolve the accumulation mode into ionic, VolatileOC, RefractoryOC, and BC mass. If coarse dust or fly ash had been a common contributor then additional procedures could be implemented to extract these components based upon their size distributions [*Clarke et al.*, 2004] but neither were identified as important during INTEX-NA. We do not include the possible changes in refractive index for heated OPC sizes arising because of volatilizing some components.

[28] The results of this procedure for examples of elevated P and BB size distributions reveal marked differences and are illustrated for two cases here as pie charts in Figure 2. The inferred P aerosol dry mass is dominated by soluble inorganic ions (79%) with about 16% VolatileOC and 4% RefractoryOC. The estimated BC is only 2% of the mass and confirms the choice of MAE for BC has little impact on determination of other constituents. The inferred BB mass fractions are quite different from those of P. The BB ionic fraction of 22% is about a factor of 4 lower than P; VolatileOC at 58% (factor of 3 higher) and RefractoryOC at 18% (a factor of 4 higher). InferredBC remains a small fraction of the total mass at 3%.

[29] We apply this approach to all thermally resolved size data for which corresponding ionic and BC estimates are available. These are stratified into BB and P categories based upon the trace gas analysis described earlier. Statistically representative composition and properties are constructed for P and BB plumes and the nonplume data. Figure 3 shows histograms of the accumulation mode mass fractions of ions, VolatileOC, RefractoryOC, Inferred BC and γ for the BB, P and nonplume cases. The differences for P and BB illustrated in Figure 2 are consistent with these histograms although there is clearly variability within each plume class. This reflects both variability in plume composition and that of the preexisting aerosol into which the plumes are mixed.

[30] The largest differences in BB and P mass fractions are for ions that dominate the mass fraction of P plumes. VolatileOC and RefractoryOC together dominate BB plumes. The typical values for BB are similar to mass fractions reported for BB in Africa [*Haywood et al.*, 2003] of 5%BC, 70%OC and 25% inorganic. Visual inspection of the nonplume histograms suggest a BB influence in approximately 20% of the data, indicating that pollution was the dominant contributor to regional aerosol properties during INTEX-NA. These differences in chemical composition are responsible for the large difference in the measured γ, or water uptake, evident in Figure 3 for the BB and P cases.

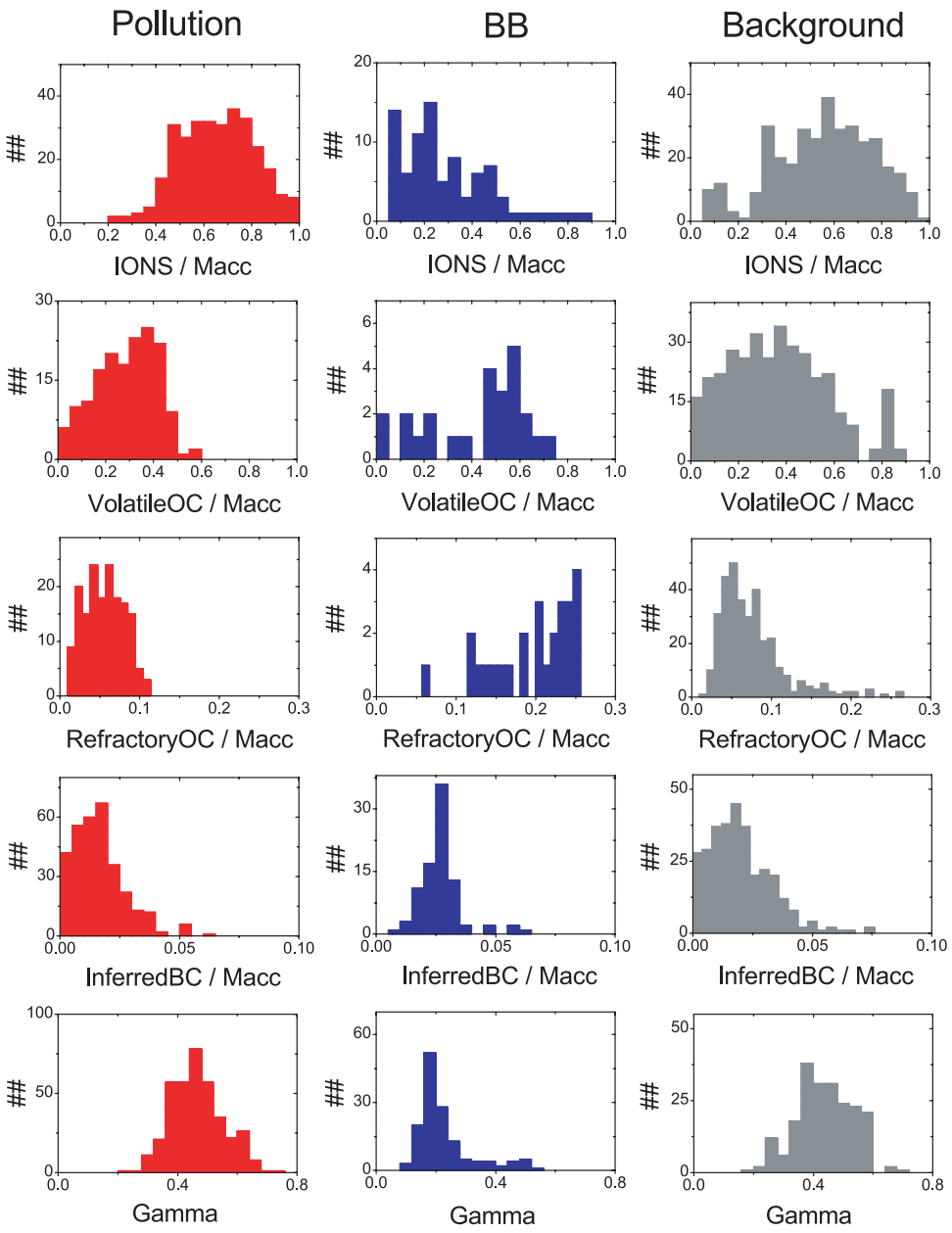

Figure 3. Histograms of mass fractions for the four indicated aerosol components obtained from the analysis described in text for P, BB, and nonplume cases. The fifth row includes measured γ associated with these cases.

[31] This characterization in terms of inferred OC fractions suggests their volatile properties are linked to the physiochemical nature of these aerosol types. However, no measurements of aerosol OC were made aboard the DC-8 and the rare comparisons with surface sites were too short and/or under conditions too inhomogeneous for direct comparison with independent measurements of aerosol OC. However, the NOAA P-3 did have a rapid measurement of CO and water soluble OC (WSOC) [*Sullivan et al.*, 2004] for flights over the eastern US during the same time period [*Sullivan et al.*, 2006]. Because the DC-8 flew in similar regions over a similar period we can compare our inferred VolatileOC versus CO measured on the DC-8 with the plot of WSOC versus CO from *Sullivan et al.* [2006] from the NOAA P-3. In-flight side-by-side comparisons of CO measurements on both aircraft differed by less than 2% making it a convenient reference.

[32] We reproduce the *Sullivan et al.* [2006] data here in Figure 4a originally reported as WSOC μgC m^{-3} for non-biomass-burning sources (grey stars, P and nonplume data) and their four BB cases (blue stars) below 2 km versus measured CO. In order to compare to their data in Figure 4a we have multiplied their carbon concentrations by 2.1 [*Turpin and Lim*, 2001] to account for the noncarbon organic mass. This allows direct comparison with our plotted VolatileOC in μg m^{-3} (for estimated density of 1.3 g cm^{-3}) against fast CO measured on the DC-8 below 2 km [*Sachse et al.*, 1987]. Our data for BB (blue), P (red)

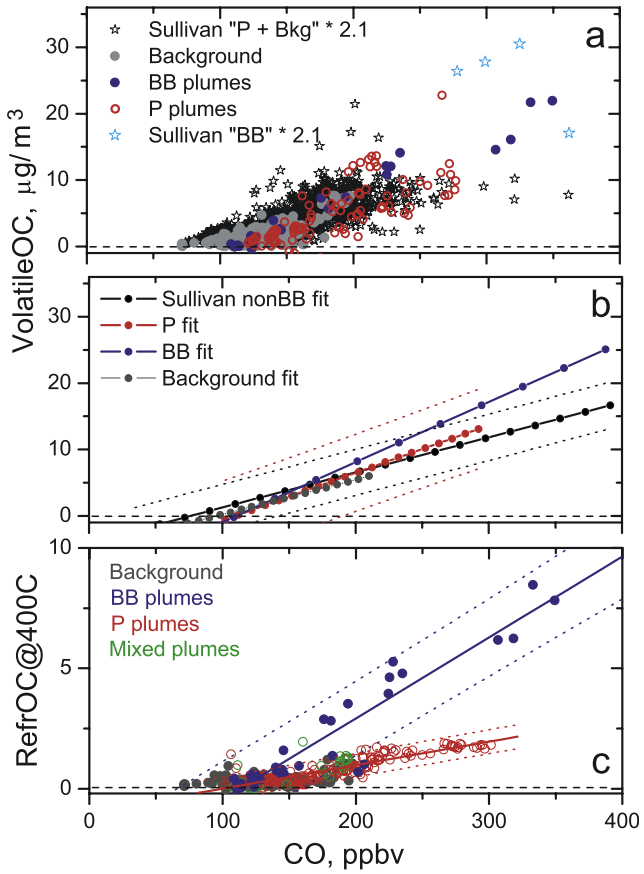

Figure 4. (a) VolatileOC mass based upon density of 1.3 g cm^{-3} versus CO for P, BB, and nonplume (background) data and *Sullivan et al.* [2006] WSOC data (stars; P + Background)) expressed as mass concentrations (see text). (b) Linear fits and 95% predictability ranges for fits to the data shown in Figure 4a. (c) RefractoryOC (ρ = 1.5 g cm^{-3}, this paper) versus CO showing distinct slopes for P and BB cases.

and background (grey) clearly overlay the *Sullivan et al.* [2006] data and show the same tendency of higher values for BB cases. For clarity, Figure 4b shows the regression lines and 95% predictability limits separately for the various data and the associated statistics are included in Table 1. We note that the scatter in our data, the overall data distribution, the slopes and the grouping of near zero VolatileOC for CO values over 100–150 ppbv are very similar to the WSOC data of *Sullivan et al.* [2006].

[33] As described earlier, this comparison required various assumptions including the density and refractive index for our OPC size data as well as density values for the indicated OC components. Moreover, these data were collected on separate aircraft sampling a large region with different objectives. This makes it difficult to establish a quantitative evaluation in spite of these similar relationships. However, we note that VolatileOC is the second most dominant component after ions for our P and nonplume cases (Figure 4) which together correspond to the *Sullivan et al.* [2006] non-BB cases. Hence a dominant fraction of what we report as VolatileOC must be their reported WSOC.

[34] Figure 4c shows our RefractoryOC has a distinct relation to CO for P and BB plumes with about four times as much RefractoryOC per CO concentration evident in the latter. Flight legs with encounters of both P and BB plumes (so-called mixed plumes) also show RefractoryOC elevated relative to P plumes. VolatileOC for BB plumes is the dominant component (see Figure 4) and its concentration relative to CO is similar to WSOC in these plumes (Figure 4). This suggests most RefractoryOC in BB plumes (Figure 4b) includes insoluble OC, in contrast to a more soluble refractory component for BB plumes in the Amazon [*Mayol-Bracero et al.*, 2002b]. Given the smaller amount of RefractoryOC in P plumes compared to VolatileOC (Figure 4) it is not clear to what extent the RefractoryOC is water soluble.

[35] Because VolatileOC appears dominated by WSOC and makes up most of the OC we can explore its relation to variability in γ. In Figures 5a and 5b, γ is plotted versus the volatile organic carbon fraction and the total ion mass fraction. In Figures 5a and 5b, γ is clearly different for the P and BB cases but shows no clear relation to the VolatileOC fraction. Even though VolatileOC is a larger fraction of total mass in BB plumes (Figures 2 and 4) the values for γ are actually lower for these plumes, indicating it is only weakly hygroscopic.

[36] We note that the PILS assessment of WSOC is under dilute conditions with significant time for dissolution and, though soluble, it is not indicative of rapid hygroscopic growth under concentrated conditions. Figure 5b shows γ is significantly related (R^2 = 0.34) to the ion mass fraction for the background data. The P data shares this dependency while BB data has generally lower γ for a given ion fraction. A plot of γ against the TotalOC fraction of accumulation mode mass (Figure 5c), clearly shows that RefractoryOC and VolatileOC both tend to reduce γ (R^2 = 0.35) as they become a larger fraction of the total aerosol mass. This confirms that the relationship found for surface

Table 1. Statistics for Line Fits in Figure 4[a]

	A	B	R^2	Std. Dev.	N
Volatile OC = A + B* CO (Figures 4a and 4b)					
2.1 * *Sullivan et al.* [2006] "P + Background"	−4.05 ± 0.22	0.053 ± 0.001	0.53	1.77	1271
P plumes	−7.88 ± 1.31	0.072 ± 0.007	0.55	2.91	89
BB plumes	−10.04 ± 0.65	0.091 ± 0.003	0.96	1.31	27
Background	−5.06 ± 0.36	0.053±0.003	0.58	1.10	266
Refractory OC = A + B* CO (Figure 4c)					
P plumes	−0.98 ± 0.07	0.010 ± 0.004	0.79	0.25	167
BB plumes	−3.81 ± 0.34	0.034 ± 0.002	0.90	0.75	36

[a]A, intercept and uncertainty; B, slope and uncertainty; R^2, correlation coefficient, Std. Dev., standard deviation; N, number of points.

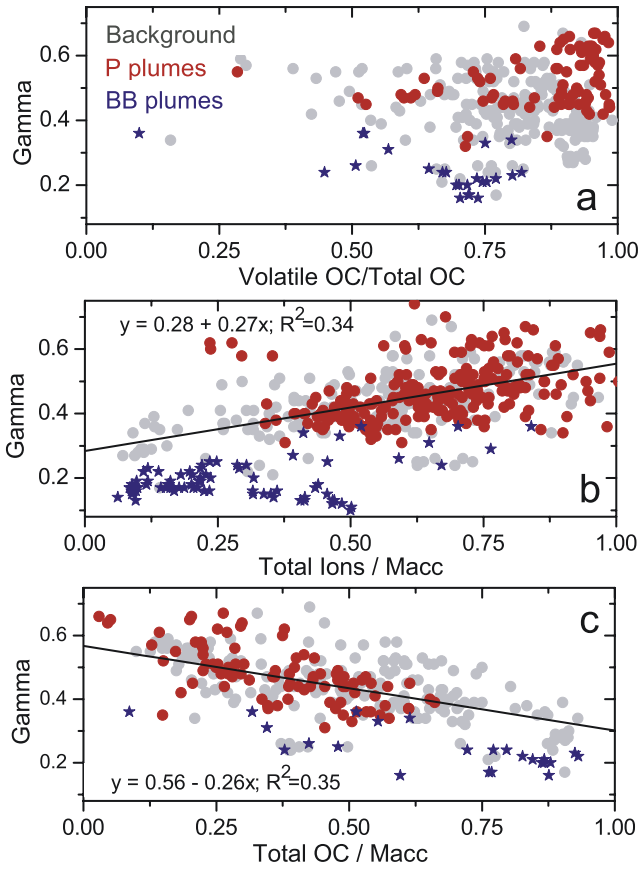

Figure 5. Plots of gamma (γ) derived from measured f(RH) against (a) the volatileOC fraction of total OC, (b) the soluble ion fraction of accumulation mode mass, and (c) the OC fraction of accumulation mode mass. Regression lines for the nonplume data only are included in Figures 5b and 5c.

observations downwind of the east coast and in our data in Asian outflow [*Quinn et al.*, 2005] also applies generally to the North American aerosol sampled during INTEX-NA.

6. Spectral Dependence of Absorption and RefractoryOC

[37] As noted in the introduction, the light scattering and light absorbing properties of the aerosol and their wavelength dependence are linked to size and composition. The wavelength dependence of absorption (absorption Angström coefficient, α_{ap}) and scattering (scattering Angström coefficient, α_{sp}) are defined as:

$$\alpha_{ap} = \ln\left(\sigma_{ap,470}/\sigma_{ap,660}\right) \Big/ \ln\left(660/470\right) \quad (2a)$$

and

$$\alpha_{sp} = \ln\left(\sigma_{sp,450}/\sigma_{sp,700}\right) \Big/ \ln\left(700/450\right) \quad (2b)$$

[38] A plot of absorption measured at 470 nm against absorption at 660 nm (Figure 6) for all the data clearly reveals an enhanced absorption for BB plumes in the shorter wavelengths, consistent with other measurements on BB aerosol [*Kirchstetter et al.*, 2004]. The tight relationship in this dependency for BB plumes confirms instrument stability for both wavelengths and implies that the greater scatter evident for P plumes is due to more variable spectral response, presumably related to a more variable physiochemistry. Histograms of this wavelength dependence for these plumes are also shown for P, BB and nonplume data. We find that α_{ap} for P is commonly near 1.1 and close to the 1.0 expected for absorbing particles that are small compared to the wavelength but consistent with values (0.7–1.1) observed elsewhere for pollution aerosol [*Kirchstetter et al.*, 2004]. Values of α_{ap} for BB peak near 2.1 and are consistent with the range of 1.2–2.2 reported by the same author for African biomass smoke. The regional nonplume cases (Figure 6c) clearly show a distribution of α_{ap} values peaking near 1.3 and with a spread suggesting a dominant P aerosol with some BB influences, also evident in the mass fraction histograms (Figure 3).

[39] The steeper wavelength dependence for BB is related to the enhanced organic fraction in the BB aerosol (Figure 3). It is of interest to determine whether the volatile

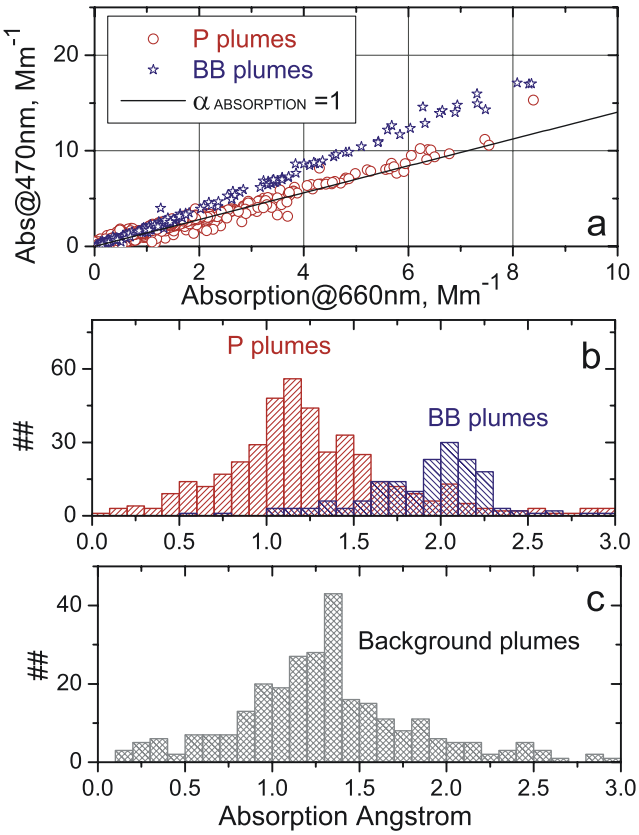

Figure 6. (a) Plot of 3-λ PSAP absorption at 470 nm against 660 nm for BB and P plumes revealing clear differences in slope. (b) Histograms of Angström coefficients for BB and P plumes and (c) histogram of nonplume data.

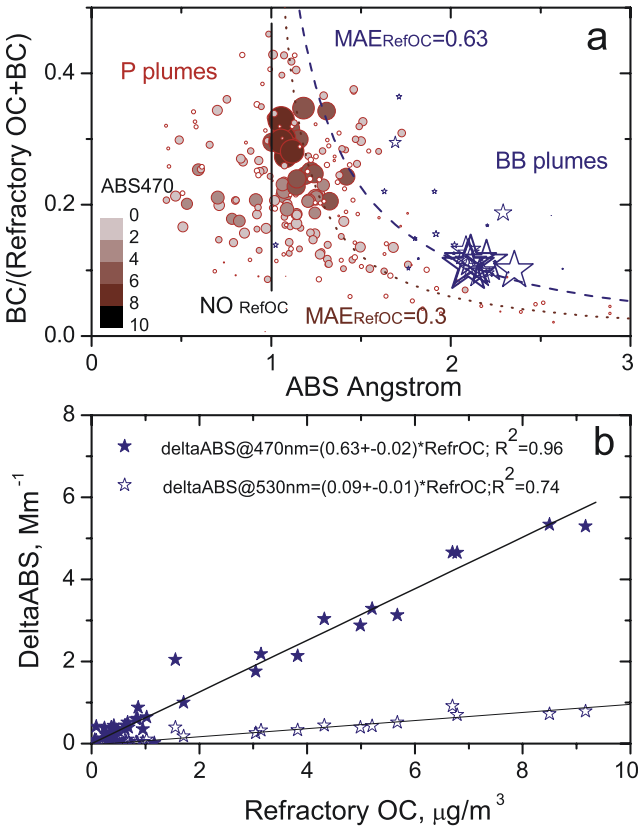

Figure 7. (a) Accumulation mode mass fraction of BC estimated from absorption at 660 nm to the sum of RefractoryOC + BC plotted against the α_{ap} for P and BB cases. Point size and darkness are proportional to total absorption at 470 nm in order to emphasize points with least measurement uncertainty. BB plumes with higher α_{ap} have highest RefractoryOC fraction, but a similar tendency is also evident in the P data. (b) Slope of enhanced absorption at 470 nm and 530 nm versus RefractoryOC in BB plume yielding an MAE of 0.63 m^2 g^{-1} for the RefractoryOC component. The dependency expected for this value is shown as the dashed line in Figure 7a along with a lower value of 0.25 that appears to fit non-BB data (dots) (see text).

or refractory organic carbon species are most responsible for the steeper wavelength dependence (Figure 7a). To do this we define BC mass as that derived using the λ^{-1} dependency from the BC estimated at 660 nm. Negligible absorption at 660 nm is assumed for RefOC. We then plot the mass ratios of BC/[RefractoryOC + BC] against α_{ap} to see if an increasing mass fraction of RefractoryOC leads to a larger α_{ap}. The size of the data points are proportional to the BC amount (also color shaded darker for higher amounts) so that the more uncertain values at low concentrations are less pronounced. Although there is considerable scatter, the α_{ap} for the P and BB cases increase as the RefractoryOC fraction of total OC increases (Figure 7a). Similar plots with RefractoryOC replaced with TotalOC or VolatileOC showed no similar trend (not shown). Hence we argue the refractory fraction of the OC is responsible for the shortwave enhanced absorption although it is not clear that our temperature defining Refractory OC is optimal for separating these components.

7. Discussion

[40] Our combined measurements of size-resolved aerosol thermal volatility, estimated BC mass from light absorption and ionic mass provide estimates of VolatileOC and RefractoryOC. These OC components comprise about 30% ± 10% of pollution plumes and about 80% ± 10% of biomass burning aerosol in plumes measured over North America during INTEX-NA. Both OC components suppressed relative light scattering (aerosol growth) under increasing humidity as their mass fractions increased. VolatileOC was shown to be related to WSOC while RefractoryOC appears to account for most enhanced absorption at shorter wavelengths in BB over North America. Hence the absorption properties of the RefractoryOC component are important to determine. Because the mass of RefractoryOC is distributed over a well-defined size range (Figure 2), it is useful to establish the mass absorption efficiency (MAE) of this component as this allows calculation of absorption from the relevant OC mass measured or present in the models.

[41] We estimate the MAE of RefractoryOC by recognizing absorption at 660 nm is dominated by BC and OC generally contributes a negligible amount at this wavelength [*Hoffer et al.*, 2005; *Kirchstetter et al.*, 2004]. We account for the BC absorption at shorter wavelengths by applying a λ^{-1} dependence for the P plumes dominated by absorbing BC (Figure 6b). If we assume the BC component in BB plumes absorbs with this wavelength dependence then the BC contribution to absorption can be estimated for all wavelengths. When subtracted from total BB absorption measured at 530 nm and 470 nm this leaves an absorption enhancement ($\boldsymbol{\Delta\sigma_{ap}}$) due to OC. On the basis of Figure 7a we argue that this is primarily due to the RefractoryOC.

[42] The resulting $\boldsymbol{\Delta\sigma_{ap}}$ data for BB plumes are shown versus RefractoryOC mass in Figure 7b. The linear slope for $\boldsymbol{\Delta\sigma_{ap}}$ versus RefractoryOC mass defines the MAE at 470 nm with a value of 0.63 m^2 g^{-1} while at 530 nm it drops to 0.09 m^2 g^{-1}. These values are small compared to the MAE for BC but the RefractoryOC present in BB aerosol can be ten times the mass of BC (Figure 3). In such cases the RefractoryOC will have about 10–15% of BC absorption at 530 nm but may equal that of BC at 450 nm. The effect of adding increasing RefOC to BC is shown as a heavy black dashed line for BB in Figure7a where the absorption values in equation (2a) have been replaced with the product of the relative mass of BC and RefOC and their respective MAE. Clearly, the line fit using the BB value for MAE does not represent the Pollution data. If a lower MAE of 0.25 is arbitrarily taken for the absorption by RefOC for Pollution we get the dotted curve that better matches the Pollution data. Hence this suggests lower values in general for the MAE of this component in pollution plumes. There is no reason MAE for the refractory OC of P aerosol should be the same as the BB value.

[43] These MAE values are based upon the 3-λ PSAP absorption, OPC volumes and the assumed density of 1.8 g cm^{-3}. While the latter are reasonable their possible

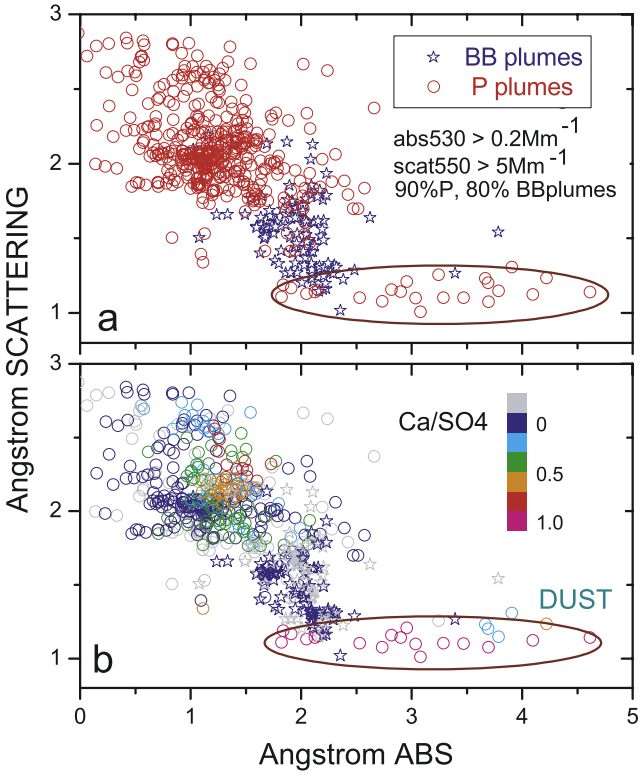

Figure 8. (a) Plot of the wavelength dependence of scattering against the wavelength dependence of absorption for P and BB plumes with anomalous P plumes circled. (b) Same as Figure 8a only color coded with Ca/SO_4 (relative units) revealing probable influence of coal fired emissions (colored cluster) and elevated dust contributions (circled) (see text). Grey points mean no Ca or SO_4 available.

uncertainty could possibly bias these estimates by as much as 20%. We also note that our RefractoryOC is operationally defined based upon the 400°C temperature separation discussed earlier. Hence the absorbing OC component may have a mass somewhat larger or smaller than we estimate here depending upon its thermal behavior near 400° as well as possible volatility of nonabsorbing components near this temperature. This thermal behavior is also likely to depend in a complex way upon fuel type and combustion conditions, as in the case of coal [e.g., *Bond et al.*, 1999b; *Bond et al.*, 2002]. Furthermore, we have treated RefractoryOC here as a separable component from BC but it is likely to be a primary emission that is absorbing and mixed with the BC at the source. As such, it may act to enhance BC absorption and/or "shield" some of the encapsulated BC from the full intensity of incident radiation [*Fuller et al.*, 1999]. Understanding such effects will require careful modeling of the effective absorption of the combined mixture.

[44] The wavelength dependence of scattering, α_{sp} is closely coupled to the size distribution. The examples of BB and P plumes shown in Figure 2 reveal BB plume aerosol sizes to be larger. If this is typical of aged BB sources, then BB plumes should be distinguishable not only by their absorption Angström coefficient but also their α_{sp}. This is evident in Figure 8a where these coefficients are plotted against each other and show a clustering of the BB and P cases. The few cases of α_{ap} below 1.0 are due in part to low absorption values (obtained from a differential measurement) and the influence of pressure and RH fluctuations on PSAP measurements. These data include σ_{ap} values as low as 0.2 Mm^{-1} that can have large uncertainties. However, after raising the threshold to 3 Mm^{-1} (not shown) the cluster behavior evident here remained unchanged although many outliers were appreciably reduced. This clustering follows form the larger size (smaller scattering Angström) and enhanced shortwave absorption (larger α_{ap}) of BB plumes relative to P. However, some apparent P data appear to be exceptions and are circled.

[45] In Figure 8b, the same data is color coded by the measured ion Ca/SO_4 ratio whenever this ion data was available. Circled data are clearly most enhanced in Ca/SO_4 and all occurred during Flight 18 over the Gulf of Mexico in an air mass coming from the south. Enhanced coarse particle volume (OPC) and coarse scattering (not shown) also confirmed the presence of a mixture of coarse dust and pollution for these cases. Increasing dust concentration lowers the α_{sp} [*Clarke et al.*, 2004] and dust has enhanced absorption at short wavelengths that exceeds those of RefractoryOC [*Patterson*, 1981]. Hence the observed behavior of these circled points makes sense and demonstrates the value of these spectral signatures for identifying aerosol types and their mixtures.

[46] The color gradient in α_{ap} within the dense P cluster in Figure 8b also reveals an elevated Ca/SO_4 ratio but the high α_{sp} above 2 indicates small particles and not dust. However, this is consistent with the high Ca/SO_4 ratio present in coal fired power plants in the eastern USA [*Anderson et al.*, 2002] and the measured fugitive emissions from such plants that often peak at sizes near 0.3 μm [*Mohr et al.*, 1996]. The displacement of this cluster from the nearby α_{ap} values having a λ^{-1} dependency characteristic of BC (cluster of blue points), probably represents the influence of brown LAC on the wavelength dependence of absorption in coal combustion plumes [*Bond et al.*, 1999b].

[47] These intensive aerosol optical properties and their link to physiochemistry and γ also influence ambient values of the aerosol single scattering albedo. Although SSA is often reported for measured dry aerosol, the ambient SSA of "wet" aerosol is essential for modeling atmospheric radiative effects and interpreting remotely sensed products. Here we show how systematic differences in size, composition and γ for the BB and P plumes lead to variability in ambient SSA. In this evaluation we assume absorbing properties are not affected by water uptake [*Nessler et al.*, 2005].

[48] The mean accumulation mode aerosol size can be expressed as an effective volume mean diameter defined by the ratio of measured OPC accumulation mode volume (Vacc) to accumulation mode number (Nacc) [*Seinfeld*, 1986]. Figure 9a shows the dry SSA versus the aerosol absorption (530 nm) and color coded with this effective diameter. A "rainbow" effect for a given absorption value reveals that dry SSA depends on size and not just absorption. The horizontal spread of data points for BB plumes with larger size (blue) shows that SSA is constant for this aerosol over a large range in absorption. This implies scattering and absorption scale together in these BB plumes while effective particle size remains the similar.

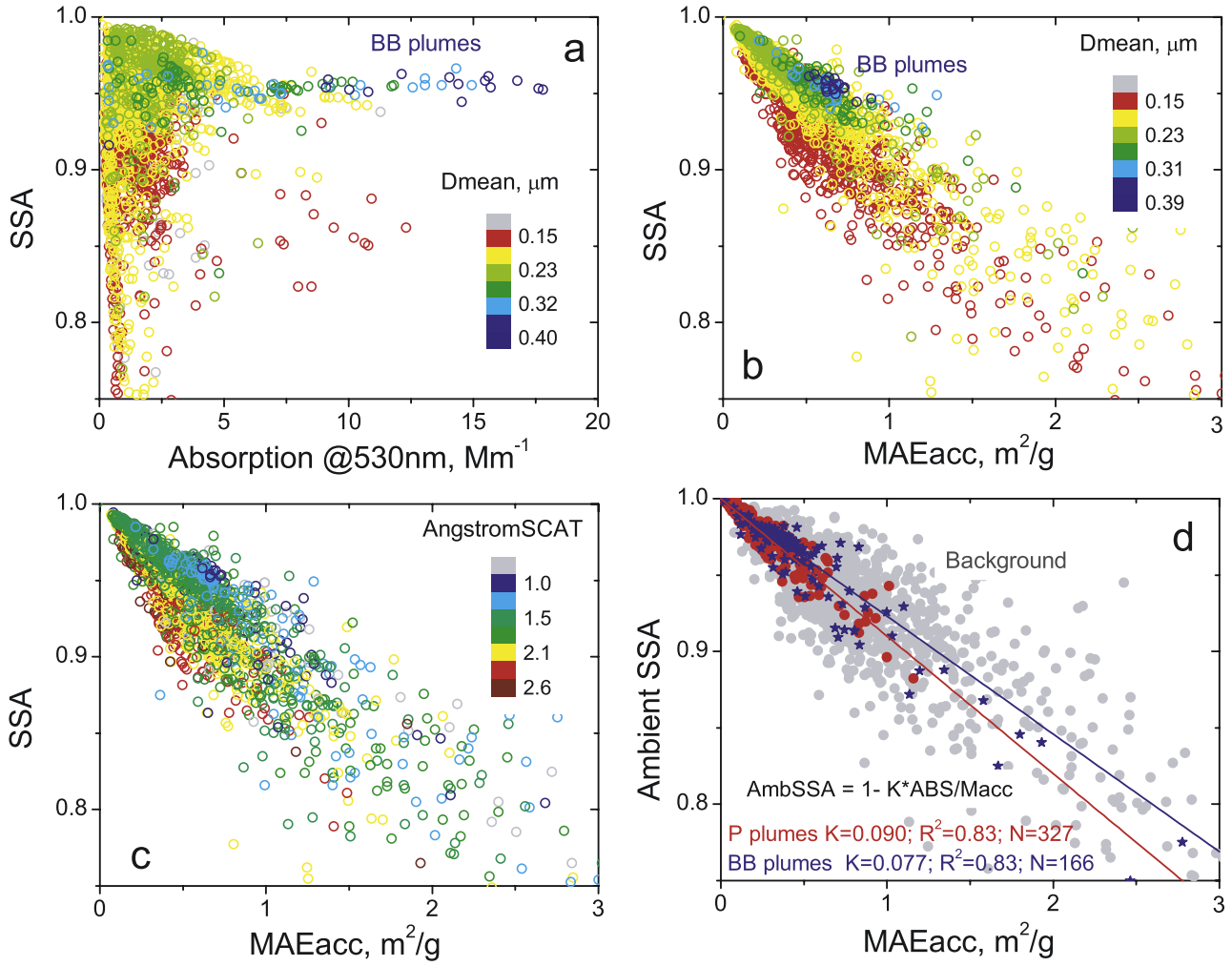

Figure 9. (a) Dry SSA versus absorption color coded with accumulation mode effective mean diameter (Dmean) revealing generally steeper slopes for smaller sizes (red) with a larger absorption to scattering. (b) Dry SSA versus MAEacc revealing "rainbow" showing a clear effect of size on dry SSA (see text). (c) Same as Figure 9b only color coded with Scattering Angström as a size index and (d) same as Figure 9c only SSA recalculated for ambient humidity and color coded by plume type.

[49] The accumulation mode SSA can be written a $(1 + \text{MAEacc/MSEacc})^{-1}$ [*Clarke et al.*, 2004] where MAEacc and MSEacc are for the accumulation mode only. For a monodisperse aerosol with an increasing absorbing component this would lead to a simple inverse dependency of SSA on MAE because the MSE will vary weakly with changes in MAE. However, MSE is quite sensitive to size such that the slope of this dependency will be influenced by the MSE through changes in effective size. In Figure 9b we plot dry SSA against the absorption per unit mass of the accumulation mode, MAEacc. This "collapses" the BB data points and "tightens" the spread of the data while preserving and enhancing the "rainbow" effect. For a given color (i.e., indicated effective diameter) an increase in MAEacc results in the expected reduction in SSA. The strongest dependency (steepest slope) is evident for the smallest sizes (red). This dependency is clear if one considers the range of SSA for particles with a particular absorption per mass (say 0.5 m^2 g^{-1}). These exhibit a dry SSA from about 0.87 to 0.97 as their effective size increases from about 0.15 to 0.4 μm. Because the scattering Angström exponent is more conventionally measured and can be sensed remotely as a size indicator (lower values indicating larger sizes, ref.) we show that it has a similar rainbow effect in Figure 9c.

[50] All of the plots in Figures 9a–9c are for the dry aerosol. However, we are most interested in the behavior of SSA under ambient conditions, $SSA_{ambient}$. This is shown in Figure 9d where we have recalculated the scattering at ambient RH based upon our measured γ. The greatest increase in $SSA_{ambient}$ is for the smaller sizes with lower dry SSA. This is in part because for a given composition or humidity-dependent diameter change, g(RH), the smaller accumulation mode sizes have significantly higher γ [*Howell et al.*, 2006b]. Also, the largest accumulation mode aerosol in INTEX-NA were measured in the BB plumes (Figure 2) having the largest OC fraction and the lowest γ (Figure 2). Both considerations imply that, for a given absorption per unit mass, $SSA_{ambient}$ increases more relative to SSA_{dry} for the smallest sizes with the largest ion fractions and changes least for the largest sizes with the lowest ion fraction. Although these dependencies are expected, the most common values are difficult to predict because of the range of

aerosol sizes, hygroscopic components, refractory constituents as well as their distributions relative to altitude (and relative humidity). Hence Figure 8d provides a representative empirical assessment of $SSA_{ambient}$ and its relation to the absorption per unit aerosol mass over North America.

[51] These data reflect the intersection of large-scale aerosol fields and humidity fields over NA during summer of 2004. Both fields may change over time or may be quite different in other regions. However, to the extent that these INTEX-NA measurements are representative of aerosol over North America, this observation is promising for models that use MSEacc, MAEacc, aerosol mass and RH to calculate ambient aerosol extinction and SSA. Figure 9d suggests the range of $SSA_{ambient}$ simulated by a model can be constrained by the regressions indicated for P and BB plumes. Models that include the absorbing aerosol component and the accumulation mode mass should obtain typical ambient SSA values indicated in Figure 9d. The results also indicate that, for the same absorption per unit mass, P plumes will have a somewhat lower $SSA_{ambient}$ values than BB plumes. The lower correlation coefficient indicated for the BB plumes is a result of the fewer data points and the greater scatter at large MAEacc for these cases.

8. Conclusion

[52] Thermal volatility of dry size distributions was used in conjunction with concurrent measured ion concentrations, BC mass estimated from measured light absorption and realistic density values to provide estimates of the OC mass concentration by difference. Heating to 400°C is effective at separating out a more volatile and refractory organic component. The relation between VolatileOC and CO was shown to be similar to that for water soluble OC (WSOC) measured on the NOAA P3-B during the same campaign, indicating that these are likely dominated by the same OC species. On the other hand, the RefractoryOC remaining at 400°C was the OC component that exhibited the short wavelength enhancement in absorption characteristic of biomass burning aerosol. It is likely that many of these condensed out near the source at temperatures above 400°C and constitute a primary emission component. The same is probably true for some the aromatics in pollution aerosol that yield enhanced shortwave absorption [*Bond et al.*, 1999b; *Schnaiter et al.*, 2006]. Enhanced shortwave absorption was not evident for the VolatileOC fraction presumably dominated by secondary aerosol formation at ambient temperatures.

[53] This rapid in situ thermal technique characterized the OC aerosol mass related fundamental physiochemical properties. This provided a surrogate OC measurement for INTEX-NA as no measurements of aerosol OC were available on the DC-8. Statistically significant differences in mass fractions of ions, VolatileOC, RefractoryOC, and BC were obtained for biomass (BB) and pollution plumes (P) independently identified by trace gases. These differences resulted in less growth under increasing RH for BB plumes due to their larger OC mass fractions. Comparison of P and BB plume properties with nonplume data (regional background) showed the latter was more strongly influenced by P and BB emissions below about 2 km but BB plumes had a greater contribution above that altitude.

[54] Multiwavelength measurements of absorption and scattering coefficients distinguished BB, P and dust influenced plumes. The absorption Angström coefficient (470–660 nm) for BB plumes had a value centered about 2.1 while that of P plumes was often near 1. Most data driving this value above 1.0 for P aerosol had an enhanced Ca/SO_4 ratio suggestive of coal fired boiler emissions. This implies absorbing RefractoryOC is also emitted from this source. Shortwave absorption in BB plumes was enhanced over that expected for BC and increased with RefractoryOC. The slope of this dependency for BB yielded a mass absorption efficiency, MAE, for this OC component of about 0.63 $m^2\ g^{-1}$ at 470 nm and dropping to 0.09 $m^2\ g^{-1}$ at 530 nm. The latter is about three times the value reported for HULIS in bulk samples at 532 nm [*Hoffer et al.*, 2004] and described by these authors as being a lower limit compared to the aerosol phase. For these BB aerosols the fraction of total absorption due to RefractoryOC was comparable in magnitude to BC at 470 nm but on the order of 10% of BC at 530 nm. Refractory OC associated with P cases was a smaller fraction of mass and more variable but appeared to have a lower MAE than BB by a factor of two or so.

[55] The RH dependence of light scattering expressed as γ was shown to depend upon composition and size in ways that were linked to spectral optical properties and chemistry, including the OC component. Smaller but more absorbing aerosol in pollution exhibited the largest values for γ while the BB aerosol exhibited the lowest γ. Under ambient RH the $SSA_{ambient}$ depended upon absorption per unit mass and the identified regressions for P and BB plumes provide useful constraints for model values of ambient SSA.

[56] **Acknowledgments.** We would like to acknowledge support of part of our team through NASA grant NNG04GB39G and NNG05GQ45H for this work. We also thank the NASA DC-8 team at NASA's Dryden Flight Research Center, California, for their mission support. We extend a special thanks to David Covert (University of Washington) for loan of the 3-λ PSAP for this study. We also thank Glen Sachse (NASA Langley Research Center) for the CO data and Rodney Weber for the WSOC data used here. This is SOEST contribution 7114.

References

Anderson, R., D. Martello, P. Rohar, B. Strazisar, J. Tamillia, K. Waldener, and C. White (2002), Sources and composition of PM2.5 at the National Energy Technology Laboratory in Pittsburgh during July and August 2000, *Energy Fuels*, *16*, 261–269.

Anderson, T., and J. Ogren (1998), Determining aerosol radiative properties using a TSI 3563 integrating nephelometer, *Aerosol Sci. Technol.*, *29*, 57–69.

Anderson, T. L., et al. (1996), Performance characteristics of a high-sensitivity, three-wavelength, total scatter/backscatter nephelometer, *J. Atmos. Oceanic Technol.*, *13*, 967–986.

Andreae, M. O., and A. Gelencser (2006), Black carbon or brown carbon? The nature of light- absorbing carbonaceous aerosols, *Atmos. Chem. Phys. Disc.*, *6*, 3419–3463.

Bates, T. S., et al. (2006), Aerosol direct radiative effects over the northwest Atlantic, northwest Pacific, and North Indian Oceans: Estimates based on in-situ chemical and optical measurements and chemical transport modeling, *Atmos. Chem. Phys.*, *6*, 1657–1732.

Bond, T. C., and R. W. Bergstrom (2006), Light absorption by carbonaceous particles: An investigative review, *Aerosol Sci. Technol.*, *40*, 27–67, doi:10.1080/02786820500421521.

Bond, T. C., T. L. Anderson, and D. Campbell (1999a), Calibration and intercomparison of filter-based measurements of visible light absorption by aerosols, *Aerosol Sci. Technol.*, *30*(6), 582–600.

Bond, T. C., M. Bussemer, B. Wehner, S. Keller, R. J. Charlson, and J. Heintzenberg (1999b), Light absorption by primary particle emissions from a lignite burning plant, *Environ. Sci. Technol.*, *33*(21), 3887–3891.

Bond, T. C., D. S. Covert, J. C. Kramlich, T. V. Larson, and R. J. Charlson (2002), Primary particle emissions from residential coal burning: Optical properties and size distributions, *J. Geophys. Res.*, *107*(D21), 8347, doi:10.1029/2001JD000571.

Bond, T. C., G. Habib, and R. W. Bergstrom (2006), Limitations in the enhancement of visible light absorption due to mixing state, *J. Geophys. Res.*, *111*, D20211, doi:10.1029/2006JD007315.

Clarke, A. D. (1991), A thermo optic technique for in situ analysis of size-resolved aerosol physicochemistry, *Atmos. Environ., Part A*, *25*(3–4), 635–644.

Clarke, A. D., et al. (2004), Size distributions and mixtures of dust and black carbon aerosol in Asian outflow: Physiochemistry and optical properties, *J. Geophys. Res.*, *109*, D15S09, doi:10.1029/2003JD004378.

Colarco, P. R., M. R. Schoeberl, B. G. Doddridge, L. T. Marufu, O. Torres, and E. J. Welton (2004), Transport of smoke from Canadian forest fires to the surface near Washington, D. C.: Injection height, entrainment, and optical properties, *J. Geophys. Res.*, *109*, D06203, doi:10.1029/2003JD004248.

Dibb, J. E., R. W. Talbot, E. M. Scheuer, G. Seid, M. A. Avery, and H. B. Singh (2003), Aerosol chemical composition in Asian continental outflow during the TRACE-P campaign: Comparison with PEM-West B, *J. Geophys. Res.*, *108*(D21), 8815, doi:10.1029/2002JD003111.

Fuller, K. A., W. C. Malm, and S. M. Kreidenweis (1999), Effects of mixing on extinction by carbonaceous particles, *J. Geophys. Res.*, *104*(D13), 15,941–15,954.

Graber, E. R., and Y. Rudich (2006), Atmospheric HULIS: How humic are they? A comprehensive and critical review, *Atmos. Chem. Phys.*, *6*, 729–753.

Haywood, J. M., S. R. Osborne, P. N. Francis, A. Keil, P. Formenti, M. O. Andreae, and P. H. Kaye (2003), The mean physical and optical properties of regional haze dominated by biomass burning aerosol measured from the C-130 aircraft during SAFARI 2000, *J. Geophys. Res.*, *108*(D13), 8473, doi:10.1029/2002JD002226.

Heintzenberg, J., and R. J. Charlson (1996), Design and applications of the integrating nephelometer: A review, *J. Atmos. Oceanic Technol.*, *13*, 987–1000.

Hoffer, A., G. Kiss, M. Blazsó, and A. Gelencsér (2004), Chemical characterization of humic-like substances (HULIS) formed from a lignin-type precursor in model cloud water, *Geophys. Res. Lett.*, *31*, L06115, doi:10.1029/2003GL018962.

Hoffer, A., A. Gelenscer, P. Guyon, G. Kiss, O. Schmidd, G. Frank, P. Artaxo, and M. O. Andreae (2005), Optical properties of humic-like substances (HULIS) in biomass burning aerosols, *Atmos. Chem. Phys. Disc.*, *5*, 7341–7360.

Howell, S. G., A. D. Clarke, Y. Shinozuka, V. Kapustin, C. S. McNaughton, B. J. Huebert, S. J. Doherty, and T. L. Anderson (2006a), Influence of relative humidity upon pollution and dust during ACE-Asia: Size distributions and implications for optical properties, *J. Geophys. Res.*, *111*, D06205, doi:10.1029/2004JD005759.

Howell, S. G., A. D. Clarke, Y. Shinozuka, V. N. Kapustin, C. S. McNaughton, S. Doherty, and T. Anderson (2006b), Influence of relative humidity upon pollution and dust during ACE-Asia: Size distributions and implications for optical properties, *J. Geophys. Res.*, *111*, D06205, doi:10.1029/2004JD005759.

Kanakidou, M., et al. (2004), Organic aerosol and global climate modeling: A review, *Atmos. Chem. Phys. Disc.*, *4*, 5855–6024.

Kirchstetter, T. W., T. Novakov, and P. V. Hobbs (2004), Evidence that the spectral dependence of light absorption by aerosols is affected by organic carbon, *J. Geophys. Res.*, *109*, D21208, doi:10.1029/2004JD004999.

Li, Q., D. J. Jacob, R. Park, Y. Wang, C. L. Heald, R. Hudman, R. M. Yantosca, R. V. Martin, and M. Evans (2005), North American pollution outflow and the trapping of convectively lifted pollution by upper-level anticyclone, *J. Geophys. Res.*, *110*, D10301, doi:10.1029/2004JD005039.

Mayol-Bracero, O. L., R. Gabriel, M. O. Andreae, T. W. Kirchstetter, T. Novakov, J. Ogren, P. Sheridan, and D. G. Streets (2002a), Carbonaceous aerosols over the Indian Ocean during the Indian Ocean Experiment (INDOEX): Chemical characterization, optical properties, and probable sources, *J. Geophys. Res.*, *107*(D19), 8030, doi:10.1029/2000JD000039.

Mayol-Bracero, O. L., P. Guyon, B. Graham, G. Roberts, M. O. Andreae, S. Decesari, M. C. Facchini, S. Fuzzi, and P. Artaxo (2002b), Water-soluble organic compounds in biomass burning aerosols over Amazonia: 2. Apportionment of the chemical composition and importance of the polyacidic fraction, *J. Geophys. Res.*, *107*(D20), 8091, doi:10.1029/2001JD000522.

McMurry, P., X. Wang, K. Park, and K. Ehara (2002), Relationships between mass and mobility for atmospheric particles: A new technique for measuring particle density, *Aerosol Sci. Technol.*, *36*, 227–238.

McNaughton, C. S., et al. (2007), Results from the DC-8 inlet characterization experiment (DICE), *Aerosol Sci. Technol.*, *41*, 136–159, doi:10.1080/02786820601184406.

Mohr, M., S. Ylatalo, N. Klippel, E. I. Kauppinen, O. Riccius, and H. Burtscher (1996), Submicron fly ash penetration through electrostatic precipitators at two coal power plants, *Aerosol Sci. Technol.*, *24*(3), 191–204.

Müller, D., K. Franke, A. Ansmann, D. Althausen, and F. Wagner (2003), Indo-Asian pollution during INDOEX: Microphysical particle properties and single-scattering albedo inferred from multiwavelength lidar observations, *J. Geophys. Res.*, *108*(D19), 4600, doi:10.1029/2003JD003538.

Nessler, R., E. Wintergartner, and U. Baltensperger (2005), Effect of humidity on aerosol light absorption and its implication for extinction and the single scatter albedo illustrated for a site in the lower free troposphere, *J. Aerosol Sci.*, *36*(8), 958–972, doi:10.1016/j/aerosolsci.2004.11.012.

Novakov, T., and C. E. Corrigan (1995), Thermal characterization of biomass smoke particles, *Microchim. Acta*, *119*(1–2), 156–166.

Patterson, E. M. (1981), Optical properties of crustal aerosol: Relation to chemical and physical characteristics, *J. Geophys. Res.*, *86*(C4), 3236–3246.

Quinn, P. K., et al. (2005), Impact of particulate organic matter on the relative humidity dependence of light scattering: A simplified parameterization, *Geophys. Res. Lett.*, *32*, L22809, doi:10.1029/2005GL024322.

Reid, J. S., R. Koppmann, T. F. Eck, and D. P. Eleuterio (2005), A review of biomass burning emissions part II: Intensive physical properties of biomass burning particles, *Atmos. Chem. Phys.*, *5*, 799–825.

Sachse, G. W., G. F. Hill, L. O. Wade, and M. G. Perry (1987), Fast-response, high-precision carbon monoxide sensor using a tunable diode laser absorption technique, *J. Geophys. Res.*, *92*, 2071–2081.

Schnaiter, M., M. Gimmler, I. Llamas, C. Linke, C. Jager, and H. Mutschke (2006), Strong spectral dependence of light absorption by organic carbon particles formed by propane combustion, *Atmos. Chem. Phys.*, *6*, 2981–2990.

Seinfeld, J. H. (1986), *Atmopheric Physics and Chemistry of Air Pollution*, 738 pp., John Wiley, Hoboken, N. J.

Shinozuka, Y., A. D. Clarke, S. G. Howell, and J. Zhou (2007), Aircraft profiles of aerosol microphysics and optical properties over North America: Aerosol optical depth and its association with PM2.5 and water uptake, *J. Geophys. Res.*, doi:10.1029/2006JD007918, in press.

Singh, H. B., W. H. Brune, J. H. Crawford, D. J. Jacob, and P. B. Russell (2006), Overview of the summer 2004 Intercontinental Chemical Transport Experiment–North America (INTEX-A), *J. Geophys. Res.*, *111*, D24S01, doi:10.1029/2006JD007905.

Stelson, A. W. (1990), Urban aerosol refractive index prediction by partial molar approach, *Environ. Sci. Technol.*, *24*, 1676–1679.

Sullivan, A. P., R. J. Weber, A. L. Clements, J. R. Turner, M. S. Bae, and J. J. Schauer (2004), A method for on-line measurement of water-soluble organic carbon in ambient aerosol particles: Results from an urban site, *Geophys. Res. Lett.*, *31*, L13105, doi:10.1029/2004GL019681.

Sullivan, A. P., R. E. Peltier, C. A. Brock, J. A. de Gouw, J. S. Holloway, C. Warneke, A. G. Wollny, and R. J. Weber (2006), Airborne measurements of carbonaceous aerosol soluble in water over northeastern United States: Method development and an investigation into water-soluble organic carbon sources, *J. Geophys. Res.*, *111*, D23S46, doi:10.1029/2006JD007072.

Turpin, B. J., and H.-J. Lim (2001), Species contributions to PM2.5 mass concentrations: Revisiting common assumptions for estimating organic mass, *Aerosol Sci. Technol.*, *35*, 602–610.

Virkkula, A., N. C. Ahlquist, D. S. Covert, W. P. Arnott, P. J. Sheridan, P. K. Quinn, and D. J. Coffman (2005), Modification, calibration and a field test of an instrument for measuring light absorption by particles, *Aerosol Sci. Technol.*, *39*(1), 68–83, doi:10.1080/027868290901963.

Weber, R. J., D. Orsini, Y. Daun, Y. N. Lee, P. J. Klotz, and F. Brechtel (2001), A particle-into-liquid collector for rapid measurement of aerosol bulk chemical composition, *Aerosol Sci. Technol.*, *35*(3), 718–727.

Wittmaack, K. (2005), Combustion characteristics of water-insoluble elemental and organic carbon in size-selected aerosol particles, *Atmos. Chem. Phys.*, *5*, 1905–1913.

B. Anderson, NASA Langley Research Center, Hampton, VA 23681, USA. (b.e.anderson@larc.nasa.gov)

V. Brekhovskikh, A. Clarke, S. Howell, V. Kapustin, C. McNaughton, M. Pinkerton, Y. Shinozuka, and J. Zhou, School of Ocean and Earth Science and Technology, University of Hawaii, Honolulu, HI 96822, USA. (tclarke@soest.hawaii.edu)

J. Dibb, Institute for the Study of Earth, Oceans, and Space, University of New Hampshire, Durham, NH 03824, USA. (jack.dibb@unh.edu)

H. Turner, Department of Chemical Engineering, University of Alabama, Tuscaloosa, AL 35487, USA. (hturner@eng.ua.edu)